Swimming against a Superfluid Flow: Self-Propulsion via Vortex-Antivortex Shedding in a Quantum Fluid of Light

Myrann Baker-Rasooli,[1] Tangui Aladjidi,[1] Tiago D. Ferreira,[2] Alberto Bramati,[1,3]
Mathias Albert,[4,3] Pierre-Élie Larré,[5,*] and Quentin Glorieux[1,3,†]
[1]Sorbonne Université, ENS Paris, Collège de France, Université PSL, CNRS, Laboratoire Kastler Brossel, F-75005 Paris, France
[2]Universidade do Porto and INESC TEC, Centre of Applied Photonics, Rua do Campo Alegre, Porto, Portugal
[3]Institut Universitaire de France (IUF), 75005 Paris, France
[4]Université Côte d'Azur, CNRS, Institut de Physique de Nice, 06200 Nice, France
[5]Université Paris-Saclay, CNRS, LPTMS, 91405 Orsay, France

(Received 23 February 2026; revised 13 April 2026; accepted 21 April 2026; published 3 June 2026)

A superfluid flows without friction below a critical velocity, exhibiting zero drag force on impurities. Above this threshold, superfluidity breaks down, and the internal energy is redistributed into incoherent excitations such as vortices. We demonstrate that a mobile, finite-mass impurity immersed in a flowing two-dimensional paraxial superfluid of light can swim *against* the superfluid current when the critical velocity is exceeded. This self-propulsion is achieved by the periodic emission of vortex-antivortex pairs downstream, which impart an upstream recoil momentum that results in a net propulsive force. Analogous to biological systems that minimize effort by exploiting wake turbulence, the impurity harnesses this vortex backreaction as a passive mechanism of locomotion. Based on a simple theoretical model, we quantitatively describe how this mechanism depends on the impurity geometry and the surrounding flow velocity. Our findings establish a fundamental link between internal-energy dissipation in quantum fluids and concepts of self-propulsion in active-matter systems and open new possibilities for exploiting quantum vortices for controlled transport at the microscale.

DOI: 10.1103/ndj1-1j89

In normal fluids, viscous drag opposes the motion of immersed impurities, so efficient motion requires mitigating energy losses due to these friction forces. In nature, a wide variety of strategies have evolved to address this constraint: bacteria and microalgae rely on chemotaxis to navigate chemical gradients [1–3], birds and fish extract energy from wavy or turbulent streams [4–6], and bio-inspired microrobots exploit similar hydrodynamic phenomena [7]. Topology also enables efficient transport in active matter [8] and even in antiferromagnets through self-propulsion of skyrmion textures [9]. In an even more striking illustration, a dead trout has been shown to passively drift upstream [10,11] by harvesting momentum from Kármán vortex streets shed in a river flow [12,13].

How do these concepts translate to quantum fluids and, in particular, can one swim in a superfluid? A superfluid has the fundamental property that, below a critical velocity, it can flow without friction, suppressing drag on obstacles. First discovered in liquid helium [14,15], superfluidity has since been observed in ultracold atomic gases [16] and, more recently, nonlinear optical media [17,18]. Above the critical velocity, superfluidity breaks down, marking the onset of dissipation. In two dimensions (2D), this phenomenon typically manifests by the nucleation of quantized vortex-antivortex pairs in the wake of a wide, high-potential impurity [19], at velocities lower than Landau's speed of sound [20–23]. While this dissipative effect is well understood for static, infinite-mass impurities, the case of a mobile, finite-mass impurity [24–27] remains largely unexplored, presenting an open question regarding its dynamical behavior in this specific 2D supercritical regime.

Over the past decade, paraxial superfluids of light [28] have emerged as a main platform for exploring complex quantum hydrodynamics in 2D [29–33]. In these systems, light propagation within a Kerr medium is governed by the 2D nonlinear Schrödinger (NLS) equation [34], an analog of the Gross-Pitaevskii (GP) equation for dilute Bose-Einstein condensates [35]. This equivalence permits the observation of 2D superfluid phenomena with classical light, encompassing, e.g., zero drag [18], vortex turbulence [22,36], and Jones-Roberts solitons [37].

In this Letter, we use the paraxial-superfluid-of-light platform, specifically realized in a hot rubidium vapor [38], to experimentally investigate the fundamental problem of a mobile impurity immersed in a 2D NLS superfluid. We develop an new optical setup to monitor the full dynamics of an all-optical impurity by simultaneously recording its trajectory along the hot atomic medium and measuring both

---

[*] Contact author: pierre-elie.larre@universite-paris-saclay.fr

[†] Contact author: quentin.glorieux@sorbonne-universite.fr

the amplitude and phase of the superfluid of light at the exit of the medium. By submitting the impurity to a transverse superfluid flow, we observe a counterintuitive effect above the critical velocity: the impurity moves upstream, in stark contrast to the downstream displacement reported in a similar experiment [18]. Phase-resolved measurements reveal that this upstream motion coincides with the periodic nucleation of vortex-antivortex pairs in the wake of the impurity, triggered when the injected flow velocity exceeds the critical speed. We show that the recoil produced by each emission event generates a counterflow that helps to propel the impurity against the superfluid current, providing a quantum-hydrodynamics analog of passive vortex-powered swimming in classical fluids. Our Letter investigates and quantifies, both experimentally and theoretically, this vortex-induced counterflow mechanism, depending critically on the impurity's radius and on the surrounding flow velocity, contrasting it with the well-established sonic drag observed in other regimes [18]. These findings establish an interesting connection between superfluid hydrodynamics and active-matter propulsion mechanisms, highlighting a fundamental, domain-independent role for vortices as momentum-transfer agents.

The propagation of a paraxial, continuous-wave laser beam through a self-defocusing local Kerr medium is governed by the 2D NLS equation for the slowly varying envelope $E(\mathbf{r}_\perp, z)$ of its complex-valued electric field,

$$i\partial_z E = \left[-\frac{\nabla_\perp^2}{2k_0} + V(\mathbf{r}_\perp, z) - k_0 n_2 |E|^2\right] E. \qquad (1)$$

In this equation, $0 < z < L$ is the propagation coordinate along the medium and $\mathbf{r}_\perp = (x, y)$ are the transverse coordinates. The in-medium propagation wave number is $k_0 = 2\pi n_0/\lambda$, where n_0 and λ are the mean refractive index and the wave length in free space, and $n_2 < 0$ is the Kerr nonlinear coefficient of the vapor, here normalized by n_0. By analogy with the GP equation of atomic superfluids, Eq. (1) can be interpreted as governing the evolution, in the effective time variable z, of the wave function $E = \sqrt{\rho}\exp(i\phi)$ of a 2D superfluid of weakly interacting photons of mass k_0. Here, ρ and $\mathbf{v} = \nabla_\perp \phi / k_0$ represent the local and instantaneous density and velocity, respectively, of this 2D superfluid of light. In this formal analogy, the speed of sound in the superfluid is defined as $c_s = (|n_2|\rho_0)^{1/2}$, where ρ_0 is the unperturbed background density at the center of the transverse light spot [31,39]. We also introduce the characteristic transverse length $\xi = 1/(2k_0^2|n_2|\rho_0)^{1/2} = 1/(\sqrt{2}k_0 c_s)$, which is the healing length of the superfluid, and the characteristic longitudinal length $z_{\mathrm{NL}} = 1/(k_0|n_2|\rho_0) = 1/(k_0 c_s^2)$, known as the nonlinear length and whose inverse corresponds to the chemical potential for the superfluid [28].

Crucially, $V(\mathbf{r}_\perp, z) > 0$ models a repulsive impurity in the superfluid, which consists of a localized linear-index depletion in the transverse x-y plane. This impurity can be mobile (i.e., of finite mass) or fixed (infinite mass) with controlled strength and width, thus allowing for the study of the impurity problem over a broad range of parameters. In nonlinear optics, such a localized change in the linear refractive index can be realized by means of an external laser beam, that we will denote the impurity beam in the following, via cross-phase modulation (XPM) [34,40].

In this Letter, we implement experimentally the superfluid model (1) for an impurity of finite mass k_i (see below). It is realized by propagating two XPM-coupled laser beams through a $L = 20$-cm-long, ^{87}Rb-vapor cell heated to 150 °C [38], as illustrated in Fig. 1(a). The superfluid beam corresponds to a $\lambda = 2\pi n_0/k_0 = 780$ nm laser beam, red detuned from the rubidium $D2$ line (~ -8 GHz). At this wave length, the warm rubidium vapor displays a substantial Kerr nonlinearity which induces effective repulsive photon interactions and therefore creates a dynamically stable superfluid [31]. The impurity beam operates at $\lambda_\mathrm{i} = 2\pi n_0/k_\mathrm{i} = 795$ nm. This produces an optical potential $V(\mathbf{r}_\perp, z) > 0$ in (1) with an effective mass k_i of the same order of magnitude as the effective mass k_0 of the superfluid photons. Accordingly, the impurity behaves as a mobile object of finite mass k_i. This impurity beam is blue detuned from the rubidium $D1$ line ($\sim +2$ GHz) to maintain its initial shape during propagation along the medium. Since both beams share the same ground state, the impurity will induce optical pumping of the atoms (locally) and therefore induces a XPM on the fluid beam. The impurity has a radius (laser waist) $\sigma \simeq 7.5\xi$ of the order of a few healing lengths $\xi \simeq 50$ μm, much smaller than the overall superfluid size in the transverse plane, $\simeq 100\xi$. By optically adjusting the relative angle between the fluid and impurity beams, we adjust, by definition of the local flow velocity $\mathbf{v}$, the incoming flow velocity v_0, here in the positive-x direction. Measured relative to the speed of sound c_s, it defines the Mach number of the flow, $\beta = v_0/c_s$ [40].

Using a dual-imaging system, we simultaneously measure the fluorescence of the fluid beam from the top and record the amplitude $\sqrt{\rho}$ and phase ϕ of the superfluid at the exit of the rubidium cell. As illustrated in Fig. 1(b), we track the impurity trajectory for a flowing superfluid ($\beta = 0.7$ on the figure) and observe a clear deviation compared to the situation where the superfluid is at rest ($\beta = 0$), indicated by the light blue line. Here we show the raw data, not corrected from the systematic displacement induced by a slight mismatch between the camera and optical axis. Corrected data are shown in Fig. 2(d). The output $\sqrt{\rho}$ and ϕ are recorded using an off-axis interferometer. Typical images are shown in Fig. 1(c), where we display the fluid amplitude $\sqrt{\rho}$ (top panels) for $\beta = 0$ and $\beta = 0.4$, together with the corresponding phase maps ϕ relative to the phase ϕ_0 in the absence of the impurity (bottom). For $\beta = 0.4$, a quantized vortex-antivortex pair is

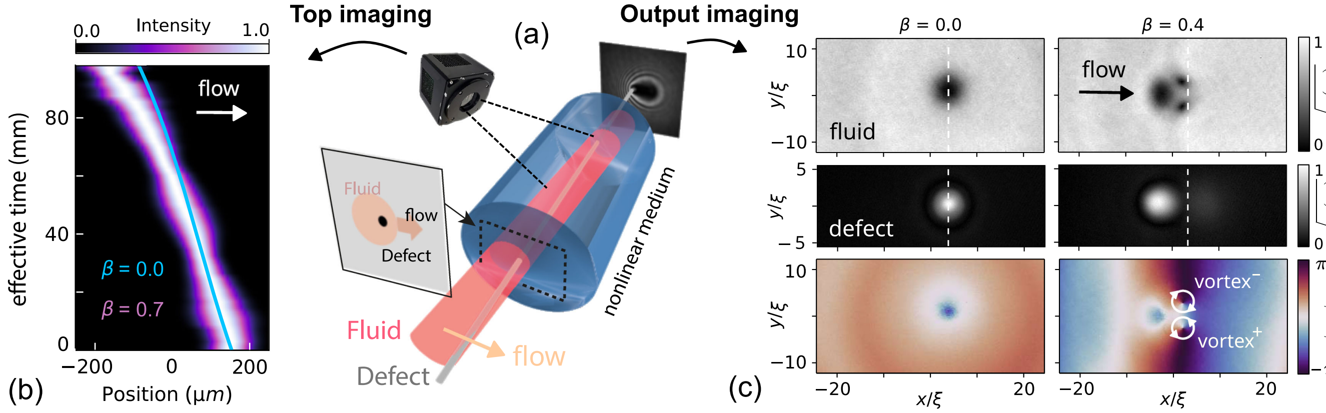

FIG. 1. Hydrodynamic flow of superfluid light past a mobile optical impurity. (a) Schematic of the experimental setup. The fluid beam is generated with a 780 nm laser beam, sent through a 20-cm-long hot rubidium-vapor cell maintained at 150 °C. The optical impurity is generated by injecting a narrower, 795 nm beam, which overlaps the fluid beam. The relative angle between the two beams controls the transverse flow velocity. (b) Intensity of the impurity beam, measured along the rubidium cell using the top imaging and a bandpass filter at 795 nm. Each segment is normalized relative to its maximum value. Raw data (before geometric correction) are presented. Light blue are the reference data corresponding to the fluid of light at rest. This dataset is used for correction of the systematic shift induced by a small camera tilt. Purple curves are the raw data for $\beta = 0.7$. A negative shift of the purple beam relative to the reference position is visible and indicates that the impurity moves upstream in the transverse plane. (c) Transverse intensity of the fluid of light at the cell output for $\beta = 0$ and $\beta = 0.4$. Top: fluid amplitudes taken with a 780 nm filter. Middle: impurity amplitudes taken with a 795 nm filter. Bottom: associated phase of the fluid. Each amplitude image is normalized to its maximum amplitude value. The vortex-antivortex pair generated downstream at $\beta = 0.4$ is highlighted with white circles centered on the $\pm 2\pi$ phase windings, respectively.

observed in the wake of the impurity, identified by detecting $\pm 2\pi$ phase windings. Importantly in the present Letter, direct access to the fluid phase allows for a measurement of the local flow velocity $\mathbf{v}(\mathbf{r}_\perp)$ [40], thus making it possible to compute the vorticity $\nabla_\perp \times \mathbf{v}$ of the superfluid. Additionally, by applying a narrow frequency filter at 795 nm, we extract the amplitude profile of the impurity, $\sqrt{\rho_\mathrm{i}} = |E_\mathrm{i}|$, at the exit of the cell, as shown in Fig. 1(c) (middle panels), revealing its displacement in the transverse plane as β increases.

Above a critical β, we observe that the impurity sheds a trailing wake of vortex-antivortex pairs orthogonal to the incident flow, as quite expected in 2D superfluids, while strikingly moving upstream, *opposite* to the incoming stream. This is illustrated in Fig. 2. Figure 2(a) shows amplitude images of the superfluid of light past the impurity for Mach numbers varying from $\beta = 0$ to $\beta = 1.1$ (top to bottom). The corresponding vorticity maps are displayed in Fig. 2(b), with the associated streamlines. The color map (saturated for visibility) highlights the downstream nucleation of paired vortices (in red, $+1$ winding number) and antivortices (blue, -1), while revealing the formation of a counterflow, in the negative-x direction, along the central axis of the vortex alley. In Fig. 2(c), we measure the x component of the local superfluid velocity in c_s units at the maximum of the impurity potential, v_x/c_s, as a function of the injected Mach number β. The horizontal solid line in black indicates 0 and the two vertical dashed lines correspond to images (i) ($\beta = 0.4$) and (ii) ($\beta = 0.6$) in Fig. 2(a). As expected theoretically for a 2D potential flow around a circular cylinder [46], the local flow velocity v_x increases linearly with β, until reaching the local speed of sound $\tilde{c}_\mathrm{s}(\mathbf{r}_\perp) = c_\mathrm{s}[\rho(\mathbf{r}_\perp)/\rho_0]^{1/2}$ at the center of the impurity, indicated by the horizontal solid line in purple. At the corresponding Mach number, $\beta \equiv \beta_\mathrm{c}$, a vortex-antivortex pair is emitted downstream, marking the transition from superfluid to dissipative flow. This is consistent with the local Landau criterion, which predicts, for impurities of large spatial extent ($\sigma \gg \xi$; $\sigma/\xi \simeq 7.5$ in our experiment), that superfluidity breaks down when the local flow velocity reaches the local sound velocity at the impurity position [47,48]. The measured critical Mach number for vortex nucleation, $\beta_\mathrm{c} \simeq 0.35$, is consistent with theoretical results for a wide impurity (see recent work [23] and references therein). A comprehensive study detailing the dependence of our β_c on the impurity parameters is left for future work.

At each vortex-antivortex emission, indicated by white circles on Fig. 2(c), the counterflow observed in Fig. 2(b) locally reduces the velocity below the local sound velocity. Assuming that the vortex pairs are emitted periodically [49], the vortex-shedding frequency $1/\Delta z$ [40] is found to linearly increase with the incoming Mach number according to $z_\mathrm{NL}/\Delta z = \sqrt{2} a\xi(\beta - \beta_\mathrm{c})$, where a is a fitting parameter with the dimensions of inverse length. The inset of Fig. 2(c) shows this frequency in units of the inverse nonlinear length, measured as a function of theβ's that mark the nucleation of the vortex pairs. It exhibits a linear trend (solid line, $a\xi \simeq 0.19$) that is consistent with similar experiments using ultracold atoms [43,49].

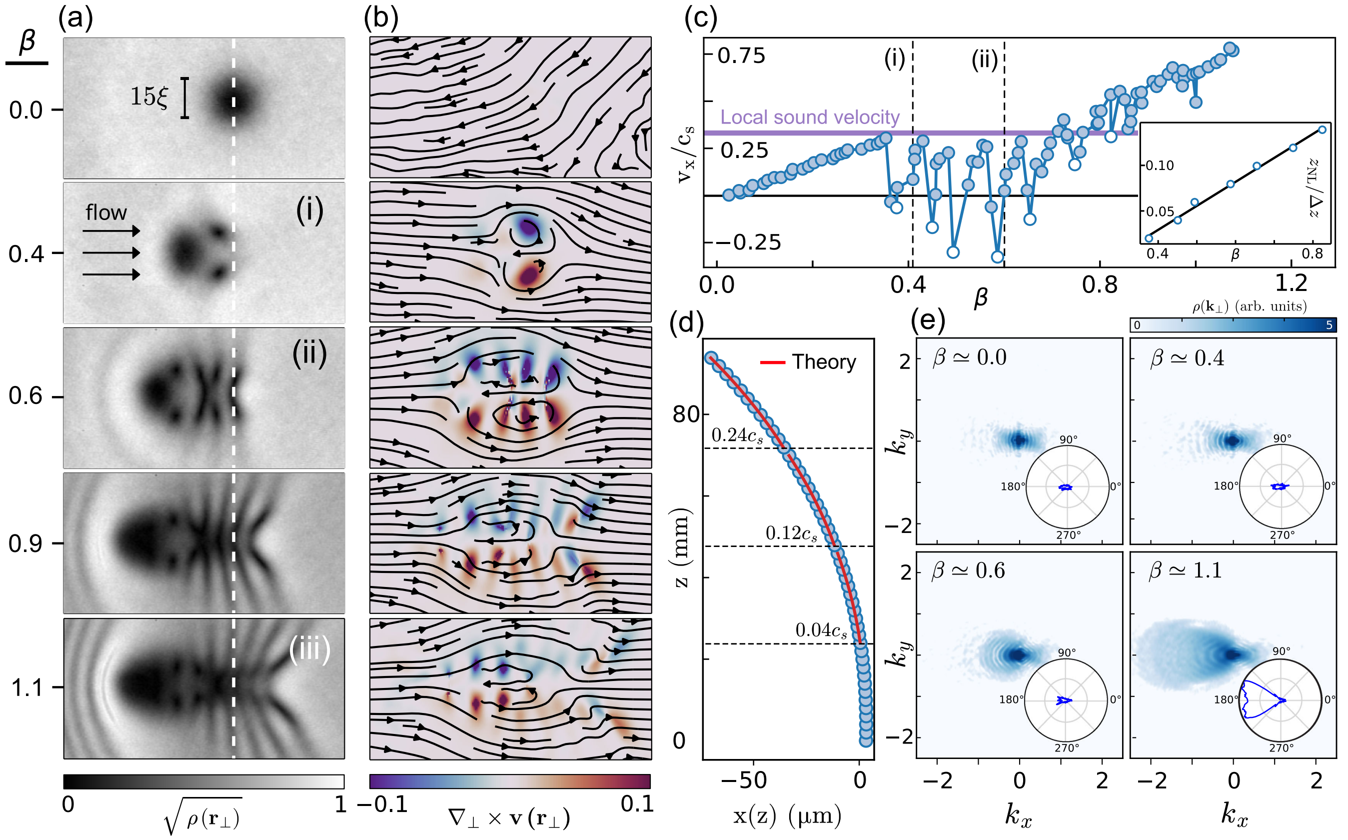

FIG. 2. Upstream motion of the impurity by vortex-antivortex shedding. (a) Output amplitude images of the fluid for increasing values of the incoming Mach number, from $\beta = 0$ (top) to $\beta = 1.1$ (bottom), with each image normalized by its maximum value. The typical radius of the impurity is $\simeq 7.5\xi$. The dashed line indicates the initial position of the impurity, highlighting upstream motion from vortex shedding. (b) Associated vorticity and streamline maps. A counterflow appears along the central axis of the vortex alley produced downstream. (c) Local flow velocity along the x axis at the position of the impurity as a function of the incoming Mach number β. When the local flow velocity reaches the local sound velocity ($\simeq 0.35c_s$, thick purple line)—which occurs at $\beta \equiv \beta_c \simeq 0.35$—the flow transitions from superfluid to normal. This change is marked by the periodic emission of vortex-antivortex pairs (white circles) and the onset of a counterflow at the center of these pairs. The two vertical dashed lines correspond to images (i) and (ii) on (a), respectively. Inset: the vortex-shedding frequency $1/\Delta z$ against β, obtained at each emission event. The solid line is obtained from a linear fit. (d) Impurity trajectory of Fig. 1(b) measured along the rubidium cell at $\beta = 0.7$ [corrected from the displacement offset of the fluid at rest shown in Fig. 1(b)]. The red parabola corresponds to the theoretical predictions [40]. (e) Momentum distribution of the fluid's excitations in the upstream region in the reference frame of the fluid for $\beta = 0$, 0.4, 0.6, 1.1. The inset of each image shows the associated polar plot.

The observed upstream motion of the impurity, evidenced by its trajectory $X(z)$ in Fig. 1(b), is directly related to the hydrodynamic force exerted by the vortices nucleated in the wake of the impurity. In Supplemental Material [40], we propose a simple model to estimate this force, based on Eq. (1). To isolate the primary mechanism, our model considers only the latest vortex pair, which we treat within a point-vortex model [44,45]. It neglects older downstream vortices, whose influence decays with distance, and averages out the transient density gradients in the wake. The trajectory $X(z)$ along the superfluid stream is found to be a parabola in the effective time z (plus linear and constant terms): $X(z) = Az^2 + O(z)$, where the acceleration A is proportional to the *negative* of the vortex-induced density imbalance $\Delta\rho = \rho_{\mathrm{down}} - \rho_{\mathrm{up}}$ between the downstream (ρ_{down}) and upstream (ρ_{up}) regions of the impurity: $A \propto -\Delta\rho$. An estimate for $\Delta\rho$ as a function of the impurity and flow parameters is given by $\Delta\rho/\rho_0 = 2\sqrt{2}(\xi/\sigma)(\beta - \sqrt{2}\xi/\sigma)$ [40]. This simplified estimate has been compared to numerical simulations of Eq. (1) and is in good qualitative agreement (not shown here for brevity). Experimentally, we operate at $\sqrt{2}\xi/\sigma \simeq 0.19$ ($\sigma \simeq 7.5\xi$), which remains below the critical Mach number $\beta_c \simeq 0.35 < \beta$ for vortex nucleation. It follows that $\Delta\rho > 0$ and thus $A < 0$, corresponding to an upstream acceleration for the impurity. This phenomenon stems from the transient formation of a density hump downstream, resulting from the upper-clockwise and lower-anticlockwise vorticity windings that effectively draw light intensity toward the rear of the impurity. This density accumulation acts as localized pressure gradient that pushes the impurity against the flow. Assuming periodic vortex emission [40], the theoretical parabolic trajectory fits the data between consecutive emission events as shown in Fig. 2(d) for $\beta = 0.7$, with a single fitting parameter providing evidence that our simplified model captures the essential physics [40].

Note that our analysis neglects other sources of drag, such as those arising from sound waves, which typically appear upstream and tend to propel the mobile impurity downstream [18,40]. This simplification is supported by Fig. 2(e), which shows the momentum distributions of the fluid's excitations at different β's in the upstream region (in the reference frame of the fluid). For $\beta < 0.8$, in the vortex-emission and self-propulsion regime, there is no significant signature of sound radiation. Evidently, sound emission begins at larger velocities, typically when $v_0 \gtrsim c_s$. This onset is signaled by a clear increase in the negative-k_x components of the momentum distributions when β is of the order of 1 and is also visible in the amplitude images of Fig. 2(a) as periodic undulations ahead of the impurity for $\beta = 0.9$ and $\beta = 1.1$.

We conclude this Letter by providing further quantitative support for the mechanisms elucidated above. With the density-weighted velocity, defined in terms of the physical velocity $\mathbf{v}$ as $\mathbf{u} = \sqrt{\rho}\mathbf{v}$, we compute the compressible component of $\mathbf{u}$, associated with sound waves, and subtract it to isolate the incompressible field $\mathbf{u}^{\mathrm{inc}}$, which is associated with vortices [40,50]. The system's net momentum is then analyzed in the downstream region, which we define from $\mathbf{u}$ as $\mathbf{p} = \int_{\mathrm{down}} d^2\mathbf{r}_\perp\, \mathbf{u}$, and focus on its x component p_x in the reference frame of the fluid [40]. We measure this observable as a function of β in Fig. 3. Data are reported as purple squares. The blue triangles and the gray inverted triangles show the incompressible (vortices) and compressible (sound waves) components of p_x, respectively, obtained from the previously used decomposition of $\mathbf{u}$. Below the critical Mach number for vortex nucleation, i.e., for $\beta < \beta_c \simeq 0.35$, the net momentum p_x is zero, as expected in this excitation-free, superfluid-flow regime. Upon exceeding β_c, p_x becomes negative (directed opposite to the incoming stream), which promotes the upstream propulsion of the impurity. This effect is clearly associated with the nucleation of vortices within the fluid, as p_x is dominated by its negative incompressible contribution.

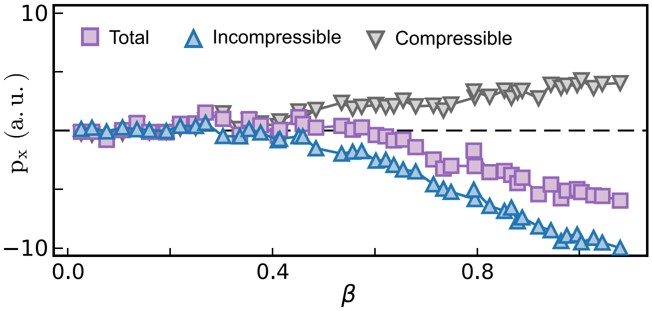

FIG. 3. Downstream x component of the net momentum of the fluid as a function of β, in the reference frame of the fluid. Purple squares, blue triangles, and gray reversed triangles, respectively, show the total, incompressible (vortex), and compressible (sound) contributions.

In this Letter, we have quantitatively investigated, both experimentally and theoretically, the dynamics of a mobile impurity in a 2D flow of superfluid light, showing that it can swim against the superfluid current as a result of the periodic nucleation of quantized vortex-antivortex pairs downstream above the critical speed. Our experimental platform provides precise control over the injected flow and enables high-resolution measurements of the full optical field, allowing one to study both the impurity dynamics and the counterflow generated by the alley of vortices emitted downstream. By employing an additional imaging system to track the impurity trajectory along the medium, we directly correlate the impurity acceleration with the emission of these vortex pairs. Most importantly, by decomposing the velocity field into its compressible and incompressible components, we show that the negative impurity's momentum originates predominantly from the vortices, drawing a direct analogy with self-propulsion in active-matter systems and classical hydrodynamics. Our observations are corroborated by a theoretical model of vortex-induced propulsion in a 2D superflow. This model provides a concise yet accurate description of the impurity's trajectory while establishing the quantitative condition required for upstream acceleration. These results open new perspectives for studying the dynamics of impurities in superfluid flows and highlight, as mentioned above, interesting connections with self-propulsion mechanisms in active-matter systems.

Acknowledgments—We acknowledge Quentin Schibler, Nicolas Pavloff, Thomas Frisch, Médéric Argentina, and Frédéric Hébert for discussions. This work has been supported by the French National Research Agency (ANR) through Grants No. ANR-21-CE47-0009 (Quantum-SOPHA) and No. ANR-24-CE47-4949 (UniQ-RingS).

Data availability—The data that support the findings of this article are openly available [51].

[1] C. Brennen and H. Winet, Fluid mechanics of propulsion by cilia and flagella, Annu. Rev. Fluid Mech. **9**, 339 (1977).

[2] L. Xie, T. Altindal, S. Chattopadhyay, and X.-L. Wu, Bacterial flagellum as a propeller and as a rudder for efficient chemotaxis, Proc. Natl. Acad. Sci. U.S.A. **108**, 2246 (2011).

[3] L. Bureau, G. Coupier, and T. Salez, Lift at low Reynolds number, Eur. Phys. J. E **46**, 111 (2023).

[4] T. Y. Wu and A. T. Chwang, Extraction of flow energy by fish and birds in a wavy stream, in *Swimming and*

Flying in Nature: Volume 2 (Springer, New York, 1975), pp. 687–702.

[5] K. D. Fausch, Profitable stream positions for salmonids: Relating specific growth rate to net energy gain, Can. J. Zool. **62**, 441 (1984).

[6] E. G. Drucker and G. V. Lauder, Locomotor function of the dorsal fin in teleost fishes: Experimental analysis of wake forces in sunfish, J. Exp. Biol. **204**, 2943 (2001).

[7] S. Palagi and P. Fischer, Bioinspired microrobots, Nat. Rev. Mater. **3**, 113 (2018).

[8] M. J. Bowick, N. Fakhri, M. C. Marchetti, and S. Ramaswamy, Symmetry, thermodynamics, and topology in active matter, Phys. Rev. X **12**, 010501 (2022).

[9] C. C. de Souza Silva, M. V. Correia, and J. C. Pena Velásquez, Emergent self-propulsion of skyrmionic matter in synthetic antiferromagnets, Phys. Rev. Lett. **135**, 086701 (2025).

[10] J. C. Liao, D. N. Beal, G. V. Lauder, and M. S. Triantafyllou, Fish exploiting vortices decrease muscle activity, Science **302**, 1566 (2003).

[11] D. N. Beal, F. S. Hover, M. S. Triantafyllou, J. C. Liao, and G. V. Lauder, Passive propulsion in vortex wakes, J. Fluid Mech. **549**, 385 (2006).

[12] T. von Kármán, *Aerodynamics* (McGraw-Hill, New York, 1963).

[13] J. E. Cooper, Aeroelastic response, in *Encyclopedia of Vibration*, edited by S. Braun (Elsevier, New York, 2001), pp. 87–97.

[14] A. J. Leggett, Superfluidity, Rev. Mod. Phys. **71**, S318 (1999).

[15] S. Balibar, The discovery of superfluidity, J. Low Temp. Phys. **146**, 441 (2007).

[16] C. Raman, M. Köhl, R. Onofrio, D. S. Durfee, C. E. Kuklewicz, Z. Hadzibabic, and W. Ketterle, Evidence for a critical velocity in a Bose-Einstein condensed gas, Phys. Rev. Lett. **83**, 2502 (1999).

[17] A. Amo, J. Lefrère, S. Pigeon, C. Adrados, C. Ciuti, I. Carusotto, R. Houdré, E. Giacobino, and A. Bramati, Superfluidity of polaritons in semiconductor microcavities, Nat. Phys. **5**, 805 (2009).

[18] C. Michel, O. Boughdad, M. Albert, P.-É. Larré, and M. Bellec, Superfluid motion and drag-force cancellation in a fluid of light, Nat. Commun. **9**, 2108 (2018).

[19] T. Frisch, Y. Pomeau, and S. Rica, Transition to dissipation in a model of superflow, Phys. Rev. Lett. **69**, 1644 (1992).

[20] W. J. Kwon, G. Moon, S. W. Seo, and Y. Shin, Critical velocity for vortex shedding in a Bose-Einstein condensate, Phys. Rev. A **91**, 053615 (2015).

[21] H. Kwak, J. H. Jung, and Y. Shin, Minimum critical velocity of a Gaussian obstacle in a Bose-Einstein condensate, Phys. Rev. A **107**, 023310 (2023).

[22] A. Eloy, O. Boughdad, M. Albert, P.-É. Larré, F. Mortessagne, M. Bellec, and C. Michel, Experimental observation of turbulent coherent structures in a superfluid of light, Europhys. Lett. **134**, 26001 (2021).

[23] J. Huynh, F. Hébert, M. Albert, and P.-É. Larré, Critical velocity of a two-dimensional superflow past a potential barrier of arbitrary penetrability, Phys. Rev. A **109**, 013317 (2024).

[24] H. Saito, Can we swim in superfluids?: Numerical demonstration of self-propulsion in a Bose–Einstein condensate, J. Phys. Soc. Jpn. **84**, 114001 (2015).

[25] L. A. Peña Ardila, G. E. Astrakharchik, and S. Giorgini, Strong coupling Bose polarons in a two-dimensional gas, Phys. Rev. Res. **2**, 023405 (2020).

[26] K. Seetharam, Y. Shchadilova, F. Grusdt, M. B. Zvonarev, and E. Demler, Dynamical quantum Cherenkov transition of fast impurities in quantum liquids, Phys. Rev. Lett. **127**, 185302 (2021).

[27] K. Seetharam, Y. Shchadilova, F. Grusdt, M. Zvonarev, and E. Demler, Quantum Cherenkov transition of finite-momentum Bose polarons, Phys. Rev. A **110**, 063306 (2024).

[28] Q. Glorieux, C. Piekarski, Q. Schibler, T. Aladjidi, and M. Baker-Rasooli, Paraxial fluids of light, Adv. At. Mol. Opt. Phys. **74**, 157 (2025).

[29] P.-É. Larré and I. Carusotto, Optomechanical signature of a frictionless flow of superfluid light, Phys. Rev. A **91**, 053809 (2015).

[30] D. Vocke, K. Wilson, F. Marino, I. Carusotto, E. M. Wright, T. Roger, B. P. Anderson, P. Öhberg, and D. Faccio, Role of geometry in the superfluid flow of nonlocal photon fluids, Phys. Rev. A **94**, 013849 (2016).

[31] Q. Fontaine, T. Bienaimé, S. Pigeon, E. Giacobino, A. Bramati, and Q. Glorieux, Observation of the Bogoliubov dispersion in a fluid of light, Phys. Rev. Lett. **121**, 183604 (2018).

[32] J. D. Rodrigues, J. T. Mendonça, and H. Terças, Turbulence excitation in counterstreaming paraxial superfluids of light, Phys. Rev. A **101**, 043810 (2020).

[33] G. Situ and J. W. Fleischer, Dynamics of the Berezinskii-Kosterlitz-Thouless transition in a photon fluid, Nat. Photonics **14**, 517 (2020).

[34] R. W. Boyd, *Nonlinear Optics* (Academic Press, London, 2020).

[35] L. Pitaevskii and S. Stringari, *Bose-Einstein condensation and superfluidity* (Oxford University Press, Oxford, 2016).

[36] M. Baker-Rasooli, W. Liu, T. Aladjidi, A. Bramati, and Q. Glorieux, Turbulent dynamics in a two-dimensional paraxial fluid of light, Phys. Rev. A **108**, 063512 (2023).

[37] M. Baker-Rasooli, T. Aladjidi, N. A. Krause, A. S. Bradley, and Q. Glorieux, Observation of Jones-Roberts solitons in a paraxial quantum fluid of light, Phys. Rev. Lett. **134**, 233401 (2025).

[38] Q. Glorieux, T. Aladjidi, P. D. Lett, and R. Kaiser, Hot atomic vapors for nonlinear and quantum optics, New J. Phys. **25**, 051201 (2023).

[39] C. Piekarski, W. Liu, J. Steinhauer, E. Giacobino, A. Bramati, and Q. Glorieux, Measurement of the static structure factor in a paraxial fluid of light using Bragg-like spectroscopy, Phys. Rev. Lett. **127**, 023401 (2021).

[40] See Supplemental Material at http://link.aps.org/supplemental/10.1103/ndj1-1j89 for additional informations as experimental details, data analysis tools, a complete description of the theoretical model and includes Refs. [18,28,35,41–45].

[41] N. Pavloff, Breakdown of superfluidity of an atom laser past an obstacle, Phys. Rev. A **66**, 013610 (2002).

[42] T. D. Ferreira, V. Rocha, D. Silva, A. Guerreiro, and N. A. Silva, Towards the experimental observation of turbulent

regimes and the associated energy cascades with paraxial fluids of light, New J. Phys. **24**, 113050 (2022).

[43] W. J. Kwon, S. W. Seo, and Y. I. Shin, Periodic shedding of vortex dipoles from a moving penetrable obstacle in a Bose-Einstein condensate, Phys. Rev. A **92**, 033613 (2015).

[44] J. Dalibard, *Fluides quantiques de basse dimension et transition de Kosterlitz-Thouless* (Lectures of the Chair Atomes et Rayonnement at Collège de France, Paris, 2016–2017).

[45] J. Skipp, J. Laurie, and S. Nazarenko, Hamiltonian derivation of the point vortex model from the two-dimensional nonlinear Schrödinger equation, Phys. Rev. E **107**, 025107 (2023).

[46] L. D. Landau and E. M. Lifshitz, *Fluid Mechanics*, 2nd ed., Course of Theoretical Physics Vol. 6 (Pergamon Press, New York, 1987).

[47] Y. Pomeau and S. Rica, Model of superflow with rotational excitations, Phys. Rev. Lett. **71**, 247 (1993).

[48] V. Hakim, Nonlinear Schrödinger flow past an obstacle, Phys. Rev. E **55**, 2835 (1997).

[49] Y. Lim, Y. Lee, J. Goo, D. Bae, and Y. Shin, Vortex shedding frequency of a moving obstacle in a Bose-Einstein condensate, New J. Phys. **24**, 083020 (2022).

[50] H. Lamb, *Hydrodynamics* (Cambridge University Press, Cambridge, England, 1932).

[51] Q. Glorieux, M. Baker-Rasooli, and T. Aladjidi Swimming against a Superfluid Flow (2026), 10.5281/zenodo.20156206.